PCCP

Accepted Manuscript

ROYAL SOCIETY OF CHEMISTRY

www.rsc.org/pccp

Functional ionic liquid for enhancement of Li-ion transfer: Effect of cation structure on charge−discharge performance of $Li_4Ti_5O_{12}$ electrode

Masahiro Shimizu,[ab] *Hiroyuki Usui,*[ab] *and Hiroki Sakaguchi*[ab*]

[a] *Department of Chemistry and Biotechnology, Graduate School of Engineering, Tottori University, 4-101 Minami, Koyama-cho, Tottori 680-8552, Japan*

[b] *Center for Research on Green Sustainable Chemistry, Tottori University, 4-101 Minami, Koyama-cho, Tottori 680-8552, Japan*

E-mail: sakaguch@chem.tottori-u.ac.jp; Fax/Tel: +81-857-31-5265

*Corresponding author.

† Electronic Supplementary Information (ESI) available: Physicochemical properties of ionic liquids, schematic illustration of gas-deposition, Raman spectra. See DOI: 10.1039/x0xx00000x

ABSTRACT

As development of high energy-density Li-ion batteries moves ahead, ensuring safety of the batteries has become increasingly important. Among unique physicochemical properties of ionic liquid, thermal stability can be one of an answer to the challenge. The use of ionic liquids, however, causes critical issues concerning kinetics of Li-ion transfer at electrode−electrolyte interface. In the present study, ionic liquids consisted of 1-((2-methoxyethoxy)methyl)-1-methylpiperidinium (PP1MEM) or 1-hexyl-1-methylpiperidinium (PP16) and bis(trifluoromethanesulfonyl)amide (TFSA) were applied to an electrolyte for Li-ion batteries, and we investigated the effect of cation structure on interfacial Li-ion transfer using $Li_4Ti_5O_{12}$ as a model electrode by means of Raman spectroscopy and electrochemical impedance spectroscopy. It was found that the ether functional group in the PP1MEM cation has the meaningful function; the cation structure reduces the electrostatic interaction between Li ion and TFSA anions in an ionic liquid electrolyte. The solvation number of TFSA anion per Li ion consequently became smaller than that in PP16-TFSA, and the less solvation number in PP1MEM-TFSA allowed the facile Li-ion diffusion in the electrolyte bulk rather than the interfacial Li-ion transfer and significantly improved rate performance. The results offer the utility of PP1MEM-TFSA as an electrolyte solvent. The knowledge obtained from this study contributes the development of next-generation Li-ion batteries having both high energy density and high safety.

KEYWORDS: $Li_4Ti_5O_{12}$; Li-ion battery; Gas deposition; Ionic liquid; Electrolyte

1. Introduction

An electrolyte, one of the three main constituents of a battery, is a key factor which governs the battery performance such as a reversible capacity and a cycle stability. Room-temperature ionic liquids have been regarded as an alternative to a conventional organic electrolyte for Li-ion batteries due to their favorable properties of non-flammability, negligible vapor pressure, wide electrochemical window, and high ionic conductivity.[1–7] The replacement of a flammable organic solvent with an ionic liquid in an electrolyte solvent can remarkably improve the safety of batteries. It is well known that ionic liquids including bis(trifluoromethanesulfonyl)amide (TFSA) anion show a low melting point and a high electrochemical stability.[8–11] Many researchers have studied the feasibility of applying the TFSA-based ionic liquids to an electrolyte solvent.[2, 12–16] The use of the ionic liquids, however, causes critical issues concerning kinetics of Li-ion transfer at the electrode−electrolyte interface.[17–20] In the TFSA-based ionic liquid electrolytes, Li ion is four-coordinated through the oxygen atoms of two bidentate TFSA anions to form $[Li(TFSA)_2]^-$ cluster in which Li ion strongly interacts with the TFSA anions by Coulomb force.[21,22] The interaction is much larger than that between Li ion and molecule solvents in an organic electrolyte system. This phenomenon limits Li-insertion into a negative electrode at low current densities in which solvation/desolvation process controls the reaction rate. In addition, charge and discharge reaction rates are controlled by Li-ion diffusion in an electrolyte bulk under high current densities. Consequently, the use of an ionic liquid electrolyte which generally has a strong electrostatic interaction in itself and has a lower diffusion coefficient of Li ion than that in an organic electrolyte results in the reason for restriction of a reversible capacity at a high rate.[19,23,24]

Recently, we demonstrated that the cycle stability of a Si negative-electrode can be markedly improved by using the ionic liquid consisting of methoxyethoxymethyl-modified piperidinium cation and TFSA anion (PP1MEM-TFSA) which we newly synthesized.[25] Furthermore, the Si electrode in the ionic liquid electrolyte exhibited the higher initial reversible-capacity than that in an ionic liquid consisting of alkyl-substituted piperidinium cation and TFSA anion (PP16-TFSA) by *ca*. 900 mA h g^{-1} at a relatively low current density of 0.12 *C* though the capacity obtained from the organic electrolyte of 1 M LiTFSA-dissolved in propylene carbonate (PC) was largest among the three kinds of electrolytes.[19] The results suggested that the cation structure of ionic liquids used as an electrolyte solvent strongly influenced the Li-insertion into the electrode.[26] We inferred that the PP1MEM cation kinetically promoted the interfacial Li-ion transfer between electrode and electrolyte. The hypothesis has remained as a matter to be discussed further. Nonetheless, the kinetic analysis of Li-insertion into the negative electrode is a quite challenge because Si absorbs Li through multi-stage alloying reactions, and the large volumetric changes in Si during charge−discharge reactions cause the severe disintegration of the electrode. We therefore focused on spinel-type $Li_4Ti_5O_{12}$ which is practically used in a negative electrode for a commercial Li-ion battery. $Li_4Ti_5O_{12}$ has been recognized as a safer active material preventing Li dendritic growth due to its higher Li insertion−extraction voltages at 1.55 V vs. Li/Li^+ than other anode materials such as graphite (C), silicon (Si), and tin (Sn). The Li-insertion mechanism is an intercalation type and the reaction proceeds based on two-phase between spinel-type $Li_4Ti_5O_{12}$ ($Li_{8a}[Li_{1/3}Ti_{5/3}]_{16d}O_4$) and rocksalt-type $Li_7Ti_5O_{12}$ ($[Li_2]_{16c}[Li_{1/3}Ti_{5/3}]_{16d}O_4$), showing a very flat plateau in charge−discharge potential curves.[27−29] Furthermore, there is little change in the lattice parameter during charge and discharge reactions, and thus achieve a high reaction reversibility and an excellent cycle stability for a long period without noticeable capacity decay.[30,31] These

characteristics are very suitable for the kinetic analysis of interfacial Li-ion transfer between electrode and ionic liquid electrolyte.

In respect to intercalation-type $Li_4Ti_5O_{12}$ and graphite negative-electrodes when using organic electrolytes, Ogumi and Abe *et al*. have clarified that the desolvation of Li ion is responsible for a large activation barrier for Li-ion transfer at the interface between electrode and electrolyte.[32,33] They concluded that the kinetics of the interfacial Li-ion transfer is influenced by a solvent molecule in an electrolyte solution, and that the activation energy reflects the facility of desolvation of Li ion from the solvent. The activation energies for the interfacial Li-ion transfer between $Li_4Ti_5O_{12}$ electrode and organic electrolyte were reported to be 48.6 kJ mol^{-1} in propylene (PC)-based electrolyte and 44.0 kJ mol^{-1} in ethylene carbonate (EC) + diethyl carbonate (DEC)-based electrolyte.[34] In the light of the above, it is considered that a higher activation energy of interfacial Li-ion transfer is required for an ionic liquid electrolyte due to a strong electrostatic interaction between Li ion and TFSA anions. However, little attention has been given to the interfacial Li-ion transfer in an ionic liquid electrolyte though there were only few reports in which commercial ionic liquids were employed.[18,26] To the best of authors' knowledge, there has been no study that tried to examine the influence of functional group attached to cation of ionic liquid on Li-insertion kinetics. In the present study, we investigated the effect of methoxyethoxymethyl (MEM) group in cation structure on the interfacial Li-ion transfer between electrode and electrolyte using a $Li_4Ti_5O_{12}$ electrode without any binder or conductive additive in terms of reaction kinetics. For the detailed analysis, PP16-TFSA including alkyl-substituted piperidinium cation with same chain length as ether-substituted one was also synthesized and applied to the electrolyte solvent. We herein discuss the above effect on the

basis of the physicochemical properties of the ionic liquids and the solvation environment of Li ions in the electrolyte solutions.

2. Experimental section

2.1. Preparation of electrolytes and electrodes

Two kinds of ionic liquids used in this study were synthesized by an organic method as previously reported[35], and are shown in Fig. 1. One is 1-((2-methoxyethoxy)methyl)-1-methylpiperidinium bis(trifluoromethanesulfonyl)amide (PP1MEM-TFSA). The other is 1-hexyl-1-methylpiperidinium bis(trifluoromethanesulfonyl)amide (PP16-TFSA). These ionic liquids were dried in a vacuum chamber at 363 K for 24 h for removing water in advance. The water contents of the ionic liquids were confirmed to be less than 50 ppm using a Karl-Fisher moisture titrator (FZ-Compact, Labconco Corporation). The ionic liquid electrolytes were prepared by dissolving the salt of lithium bis(trifluoromethanesulfonyl)amide (99.9%, LiTFSA) in each one at a concentration of 1.0 mol dm^{-3} (M). For comparison, we used the organic-based electrolyte of 1.0 M LiTFSA-dissolved in propylene carbonate (Kishida Chemical Co., Ltd.). The preparation of the electrolytes was performed within a purge-type glove box (DBO-2.5LNKP-TS, Miwa MFG) filled with an argon atmosphere from which oxygen and water had been completely removed. The glove box maintained a dew point below −100 ^{o}C and an oxygen content below 1 ppm.

$Li_4Ti_5O_{12}$ thick-film electrodes were prepared by a gas-deposition method using a commercial $Li_4Ti_5O_{12}$ powder (99%, Aldrich) with a diameter of *ca*. 100 nm.[16,36] The schematic diagram of the apparatus for gas-deposition and the detail conditions are illustrated in Fig. S1 in ESI†.

2.2 Characterization and Electrochemical measurement

The thickness and surface morphology of the deposited $Li_4Ti_5O_{12}$ film on the Cu substrate was investigated through the use of confocal laser scanning microscope (CLSM, VK-9700, Keyence).

The apparent Li-ion transference number (t_{Li+}) was determined by combination measurements consisted of ac impedance and dc polarization using an electrochemical analyzer (CompactStat, Ivium Technologies).[37−39] A symmetric cell of [Li metal | ionic liquid electrolyte | Li metal] was applied for the electrochemical measurement. A polypropylene film having pores with a dimeter of 70−240 nm was soaked in the electrolytes and was used as the separator. The frequency range of the impedance analysis was 100 kHz−100 mHz, and the dc polarization at 10 mV was performed to monitor a steady current for 8 h at 303 K.

To analyze an average solvation number of TFSA anion per Li ion in the ionic liquid electrolytes, Raman spectroscopy system (NanofinderFLEX, Tokyo Instruments, Inc.) with 532 nm line of Nd:YAG laser was used at room temperature. In order to avoid an effect of water in air, we put the electrolyte solution into a quartz cell, and tightly sealed in it within an argon atmosphere.

We fabricated 2032-type coin cells consisting of a $Li_4Ti_5O_{12}$ thick-film electrode as the working electrode, Li foil (99.90%, thickness: 1.0 mm, Rare Metallic) as the counter electrode, electrolyte, and propylene-based separator. The area of the $Li_4Ti_5O_{12}$ film and Li sheet were 0.2 cm^2 and 1.90 cm^2, respectively. To evaluate the effect of cation structure in the ionic liquids on the electrode performance, a rate capability test was carried out using an electrochemical measurement system (HJ-1001 SD8, Hokuto Denko Co., Ltd.) in the potential range between 1.00 and 3.00 V vs. Li/Li^+ at 303 K.

Electrochemical impedance spectroscopic (EIS) analysis using a three-electrode type cell was performed at 1.55 V vs. Li/Li^+ in the frequency range of 100 kHz−100 mHz with an amplitude of 5 mV. The EIS measurement was conducted at various temperatures from 298 to 328 K per 5 K to determine an apparent activation energy of interfacial Li-ion transfer between the $Li_4Ti_5O_{12}$ electrode and the ionic liquid electrolytes. Before the EIS measurement, the electrode was once cycled and charged (lithiated) up to 1.55 V vs. Li/Li^+ at 0.1 C (17.5 mA g^{-1}), and then was kept at the potential for 20 min. Two electrode-type cell was applied only when an activation energy in an organic electrolyte was evaluated.

3. Results and discussion

3.1. Characterization of ionic liquid electrolytes

To reveal the effect of cation structure on Li-ion transfer in the ionic-liquid electrolyte bulk, we evaluated the apparent Li-ion transference number (t_{Li+}) in each of the electrolyte solution by means of combination measurements consisted of ac impedance and dc polarization using a symmetric cell of [Li metal | ionic liquid electrolyte | Li metal] at 303 K. Electrochemical impedance spectroscopic (EIS) analysis for the cell was conducted to measure electrolyte bulk resistances (R_{bulk}) and charge transfer resistances (R_{ct}) at the initial state (Fig. 2a and 2b). The impedance of the cell was normalized by using the sum of areas of two Li electrodes. In the respective Nyquist plots, one semicircle which denotes R_{ct} was confirmed. The resistance is derived from the interfacial Li-ion transfer between the Li metal and the ionic liquid electrolyte. The values were analyzed using an equivalent circuit shown in Fig. 2c. Then, a polarization voltage of 10 mV (ΔV) for 8 h was applied to monitor an initial current and a steady-state

current. After the steady-state current ($Li \rightleftarrows Li^+ + e^-$) was confirmed (Fig. 2d), EIS measurement was conducted to determine the t_{Li+} according to the following equation:[37–39]

$$t_{Li+} = \frac{I(\infty)R_{bulk}(\infty)[\Delta V - I(0)R_{ct}(0)]}{I(0)R_{bulk}(0)[\Delta V - I(\infty)R_{ct}(\infty)]} \qquad (1)$$

where $I(0)$ and $I(\infty)$ are the initial state and steady-state currents, respectively. It should be noted that this equation (1) reported by Vincent and Bruce can be applied only to the evaluation for transference number of a cation with a valence "+1" in an electrolyte bulk.[37] As for ionic liquid electrolytes in which Li ions are inevitably solvated by anions to form negatively charged $[Li(TFSA)_x]^{1-x}$, the determination of transference number of Li ion requires the ratio of self-diffusion coefficient of cation species measured using pulsed-field gradient spin-echo NMR. Therefore, the transference numbers evaluated in the present study is apparent values and have no physical meaning. We will strictly investigate the transference number in a future study. The apparent transference number and measured values for the parameters are summarized in Table 1. The smaller value of R_{bulk} in PP1MEM-TFSA is due to its higher ionic conductivity (Fig. S2 and Table S1, ESI†), and the lower value of R_{ct} indicates a smooth Li-ion transfer at the Li metal and the ionic liquid electrolyte. The calculated t_{Li+} in the respective electrolytes were 0.32 for 1 M LiTFSA/PP1MEM-TFSA and 0.07 for 1 M LiTFSA/PP16-TFSA.

In organic electrolytes generally used for Li-ion batteries, Li-salt ionizes to be stabilized by solvation of solvent molecules to Li ion. On the other hand, because ionic liquids do not contain any neutral molecules, Li ion therefore undergoes coordination from anions of the ionic liquid to stabilize itself.[21,22] Since the counter anion of the ionic liquids used in this study is TFSA anion,

Li ions are inevitably solvated by the TFSA anions to form the $[Li(TFSA)_x]^{1-x}$ complexes due to the strong electrostatic interaction generated between the Li ion and the TFSA anions. The symbol "x" denotes the solvation number, which significantly influences on the kinetics of the Li-ion transfer at the electrode–electrolyte interface.[18,40,41] For a quantitative evaluation of the solvation number in two kinds of the ionic liquid electrolytes with the different cation structure, Raman spectroscopic measurements to electrolyte solutions of $(LiTFSA)_x(PP1MEM\text{-}TFSA)_{1-x}$ and $(LiTFSA)_x(PP16\text{-}TFSA)_{1-x}$ (x = 0, 0.05, 0.10, 0.15, 0.20) were performed in accordance with the literatures reported by Lassègues or Balducci *et al*.[42,43] Fig. 3 compares Raman spectra of the electrolyte solutions in the wavenumber range from 730 to 760 cm^{-1}. Although these spectra appear to be the same in a wide range (Fig. S3, ESI†), the PP1MEM-TFSA system is distinctly different from the PP16-TFSA system (Fig. S4, ESI†). The intense bands located at 742 cm^{-1} in all cases are ascribed to the CF_3 bending vibration coupled with the S−N stretching vibration of the TFSA anion.[40] The band means the existence of *free* TFSA anions ($TFSA^-_{free}$), that is, TFSA anions in the electrolyte solutions do not interact with Li ions and do not behave as a ligand for forming the $[Li(TFSA)_x]^{1-x}$ complex. In other words, the TFSA anions interact with dissociated cations (counter cations) of the respective ionic liquids. On the other hand, the additional band which is observed as a shoulder appeared at around 748 cm^{-1} in the case of presence of LiTFSA-salt (molar fraction: $x \leq 0.05$). This result indicates that Li ions were solvated by the TFSA anions to form the $[Li(TFSA)_x]^{1-x}$ complexes owing to the electrostatic interaction, and the additional band at 748 cm^{-1} here is defined as TFSA anions interacting with Li ion ($TFSA^-_{solv}$). All of the Raman spectra were deconvoluted into the two components including the $TFSA^-_{free}$ and the $TFSA^-_{solv}$ using a Gaussian function. In both the system, the band intensity of $TFSA^-_{free}$ (742 cm^{-1}) decreased with increasing LiTFSA concentration. Contrariwise, the increase in the

intensity for $TFSA^-_{solv}$ (748 cm^{-1}) was confirmed as the molar fraction of x is large. Note that the increase ratio of $TFSA^-_{solv}$ in the PP1MEM-TFSA system was smaller than that in the PP16-TFSA system, which shows that the interaction between Li ions and surrounding TFSA anions in the $(LiTFSA)_x(PP1MEM\text{-}TFSA)_{1-x}$ solutions is weaker in comparison to that in the $(LiTFSA)_x(PP16\text{-}TFSA)_{1-x}$ solutions. Fig. 4 depicts plots of $I_{solv}/(I_{free} + I_{solv})$ as a function of molar fraction (x) of LiTFSA for the electrolyte solutions, leading to the determination of an average solvation number of TFSA anions per Li ion.[42,43] The I_{free} and I_{solv} stand for the Raman intensities of $TFSA^-_{free}$ and $TFSA^-_{solv}$, respectively. The slope of dashed line represents to an average solvation number (N_{TFSA} = 1~3) as a guide. Comparing slopes obtained from plots of the respective intensity ratios, it was found that the average solvation number of TFSA anions is 1.56 for the PP1MEM-TFSA system and 2.40 for the PP16-TFSA system. The values given from the Raman measurements clearly show that the solvation environment is greatly affected by the functional group attached with cation of ionic liquid. In the case of using commercially available ionic liquids (*e.g.* PP13-TFSA: *N*-methyl-*N*-propylpiperidinium bis(trifluoromethanesulfonyl)imide and EMI-TFSA: 1-ethyl-3-methylimidazolium bis(trifluoromethylsulfonyl)imide), the solvation number generally results in "2".[21] It is well known that an ionic liquid having a cation with long alkyl chains behaves as a cationic surfactant and the cation forms an aggregation like a micelle whose hydrophobic parts are arranged inward. Kunze *et al*. studied the aggregation behavior of pyrrolidinium-based ionic liquids (Py1x, x = 3~8) with TFSA anion by means of NMR relaxation and Raman spectroscopic measurements. The difference calculated by subtracting spin-lattice relaxation rate from spin-spin relaxation rate in the ionic liquids became larger than 0 when the side chain length is longer than three (propyl), which indicates that the Py1x (x = 4~8) cations tend to aggregate. Additionally, in Raman spectra

with the presence of LiTFSA-salt, the band intensity associated with the interaction between Li ion and TFSA anions increased and the solvation number grew with increasing side chain length. This is because the aggregation degree of Py1*x* cations gradually enlarged.[44] In view of the aggregation effect, it is suggested that the interaction between PP16 cations and TFSA anions weakened. Thereby allows Li ions to be strongly trapped by the TFSA anions. This is probably considered as the reason why the average solvation number in the PP16-TFSA system became larger than that in the PP1MEM-TFSA system. By contrast, the PP1MEM cation has two negatively-charged oxygen atoms as an ether functional group (methoxyethoxymethyl) in its structure. It is inferred from the characteristics that the functional group has the ability of attracting Li ions through its lone-pair electrons. For example, an organic solvent of 1,2-dimethoxyethane (DME; $C_4H_{10}O_2$), same molecular frame as the methoxyethoxymethyl group, forms a $[Li(DME)_2]^+$ complex with Li ion via the two oxygen atoms at a certain molar ratio (Fig. S5, ESI†). In the case of the ionic liquid electrolyte, however, the phenomenon which the oxygen atoms in the functional group attract only Li-ion is unlikely in light of a repulsive force between positive Li ion and positively-charged PP1MEM cation. Tsuzuki *et al*. reported the following on the basis of ab initio molecular calculations: *N*,*N*-diethyl-*N*-methyl-*N*-(2-methoxyethyl)ammonium (DEME) cation with an electron withdrawing group forms a stable complex with LiTFSA complex rather than Li cation. The TFSA anion in the LiTFSA complex plays a key role to screen the repulsive interaction between Li caion and DEME cation.[45] Allowing for the results, it is considered that the PP1MEM cation attracts Li-ion binding with TFSA anion through the two oxygen atoms in its ether side chain to form PP1MEM-LiTFSA complex (Fig. S6, ESI†). As a result of the attractive force induced by the negatively-charged oxygen atoms in the PP1MEM cation, the average solvation number of TFSA anions in the

PP1MEM-TFSA system appears to be less than two and smaller than that in the PP16-TFSA system. The fact that the solvation number becomes smaller means that Li ions in PP1MEM-TFSA are relatively free from the constraint generated by the electrostatic interaction.

3.2. Effect of cation structure on Li-insertion/extraction property of $Li_4Ti_5O_{12}$ electrode

Fig. 5a and 5b show XRD pattern and Raman spectrum of the film prepared by gas-deposition using a $Li_4Ti_5O_{12}$ powder (inset image) on a Cu substrate. All of the peaks with the exception of the Cu current collector are attributed to lithium titanium oxide ($Li[Li_{1/3}Ti_{5/3}]O_4$) with a spinel framework structure ($Fd\bar{3}m$ space group).[27] Sharp peaks located at 233, 434, and 670 cm^{-1} in the Raman spectrum are assigned to the vibrations of crystalline lattice of $Li_4Ti_5O_{12}$ such as F_{2g}, E_g, and A_{1g} phonon modes.[29] Results obtained from the XRD and Raman measurements indicate that the film prepared by gas-deposition was composed of pure $Li_4Ti_5O_{12}$ without any impurity, and that its composition was unchanged during the film formation. Fig. 5c displays an optical image of the $Li_4Ti_5O_{12}$ electrode and a three-dimensional height profile analyzed by CLSM. The difference in the level between the substrate and the film formed by using a mask was *ca*. 36 μm, which corresponds to the thickness of the deposited active-material layer. We successfully obtained the $Li_4Ti_5O_{12}$ thick-film electrode with a thickness of several tens of micro-meters which does not contain any binder or conductive additive. It is thus possible to directly observe electrochemical reactions at the interface between the $Li_4Ti_5O_{12}$ and the ionic liquid electrolytes.

For exploring the benefits granted by the less solvation number of TFSA anions to Li ion, galvanostatic charge−discharge tests were conducted. Fig. 6 represents rate capabilities of the electrodes in the piperidinium-based ionic liquid electrolytes at various *C*-rates from 0.1 *C* (17.5 mA g^{-1}) to 20 *C* (3500 mA g^{-1}). In the rate performance tests from 0.1 *C* to 20 *C*, both charge

and discharge were conducted at the same current densities, and the geometric current density of 1.0 *C*-rate corresponds to 0.13 mA cm^{-2}. For comparison, the performance in an organic electrolyte using PC was also shown. At the low current density (*e.g.* 0.1 *C* and 0.2 *C*), PP1MEM-TFSA delivered a high discharge (Li-extraction) capacity than 170 mA h g^{-1}, which is comparable to that in the organic electrolyte. The notable point is that the $Li_4Ti_5O_{12}$ electrode in PP1MEM-TSFA exhibited the larger capacities than those in PP16-TFSA even at the low *C*-rates where an influence of concentration polarization on charge−discharge property is reduced. The result indicates that the Li-insertion/extraction capacities in the ionic liquid electrolytes are greatly affected by the solvation environment of Li ion in the respective electrolytes. When the current density was raised from 0.2 *C* to 0.5 *C*, the reversible capacity in PP16-TFSA dropped down from 143 mA h g^{-1} to 82 mA h g^{-1} with a retention of 57%. Then, the clear polarizations for charge−discharge processes appeared in the electrolytes (Fig. 7). At a high rate in which mass transport of Li ion dominates an electrochemical reaction, the charge−discharge reaction rate are controlled by Li-ion diffusion in the electrolyte solution. The poor rate performance in PP16-TFSA is presumably due to both the slow kinetics of interfacial Li-ion transfer and the low Li-ion diffusion derived from the ionic liquid electrolyte. Whereas, the electrode in PP1MEM-TFSA yield a 90% capacity of the first capacity at 0.5 *C*, and only a capacity of 16 mA h g^{-1} was decreased. Furthermore, the superiority observed in PP1MEM-TFSA became marked at a relatively high rate, as we expected; a capacity of 125 mA h g^{-1} equivalent to more than the triple of the capacity in PP16-TFSA was attained at 1.0 *C*. Li-insertion reaction into a $Li_4Ti_5O_{12}$ electrode in an ionic liquid electrolyte takes place after the following elementary steps: (i) Li-ion (solvated by TFSA anions) migration/diffusion in the electrolyte bulk, (ii) desolvation of $[Li(TFSA)_x]^{1-x}$ and Li-ion transport across the inner Helmholtz plane formed by a cation

accumulation at the interface between the electrode and the ionic liquid electrolyte. Because of the strong electrostatic interaction between Li ion and TFSA anions[19], the diffusion in the electrolyte bulk and the reaction for desolvation of the TFSA anions from the Li ion becomes slow. These phenomena limit charge−discharge capacities. As we described above, the average solvation numbers of TFSA anions are 1.56 for the PP1MEM-TFSA system and 2.40 for the PP16-TFSA system. Given the correlation between the solvation number and the rate capabilities, we assumed that either the Li-ion diffusion in the electrolyte bulk or the kinetics of interfacial Li-ion transfer depends on the solvation environment of Li ions such as the solvation number of TFSA anions.

The EIS analyses were carried out for the $Li_4Ti_5O_{12}$ electrodes in the ionic liquid electrolytes with different cation structure to discuss which factor affects charge−discharge rate performance by investigating an activation energy of the interfacial Li-ion transfer. Fig. 8a depicts a typical Nyquist plot of a negative electrode at the charge (Li-inserted) state with little influence of a surface layer, and the Nyquist plot composed of one semicircles in a high frequency and a straight line with a slope of approximately 45^o in a low frequency region. In general, these components are interpreted as following: the first semicircle (R_{ct}) originates from the interfacial Li-ion transfer processes which includes the desolvation of $[Li(TFSA)_x]^{1-x}$, the Li-ion transport in an electrical double layer and/or a surface layer induced by decomposition of electrolyte. The straight line in the low frequency is derived from the solid-state diffusion of Li (Z_w). At the Nyquist plots in the PP1MEM-TFSA and PP16-TFSA systems (Fig. 8b), we could observe the components mentioned above. The each resistance was analyzed using the equivalent circuit shown in Fig. 8a. The constant phase element (CPE) was employed in place of capacitance (C) for taking into account the roughness of the electrode surface. To examine the kinetics of the Li-

insertion reactions in the respective electrolytes, we monitored the temperature dependence of the interfacial Li-ion transfer resistance in the range from 298 K to 333 K.[34] We confirmed that the resistances obviously decreased with increasing temperature. In addition to this, the inverse of the resistances as a function of reciprocal temperature showed Arrhenius-type behavior (Fig. 8c). The inverse of the resistances (interfacial conductivities) obeys the Arrhenius-type equation:

$$\frac{1}{R_{ct}} = A\exp(-\frac{E_a}{RT}) \qquad (2)$$

where the symbol A, E_a, R and T denote frequency factor, activation energy, gas constant, and absolute temperature, respectively. The apparent activation energy for the interfacial Li-ion transfer can be determined by the slope of the Arrhenius plots.[33] Abe *et al*. reported that the activation energy for the interfacial Li-ion transfer between $Li_4Ti_5O_{12}$ thin film and ionic liquid electrolyte showed about 70 kJ mol^{-1} without depending on cation species.[18] On the other hand, in the other literature, they demonstrated that the activation energy estimated from Li-ion transfer at the lanthanum lithium titanate (LLT)/ionic liquid electrolyte interface using a four-electrode electrochemical cell was different with cation species consisting ionic liquids.[17] For example, the activation energy at the LLT/EMI-TFSA interface is lower than that at LLT/PP13-TFSA by 10 kJ mol^{-1}, and they described the reason that the interaction between Li ion and TFSA anion is more weakened by cation-anion interaction of imidazolium-based ionic liquid than by that of piperidinium-based ionic liquid. From this points, it is no wonder that the activation energy obtained from the $Li_4Ti_5O_{12}$ electrode/PP1MEM-TFSA interface is smaller than that from the $Li_4Ti_5O_{12}$ electrode/PP16-TFSA interface. Contrary to our expectation, the activation energy calculated from the R_{ct} was same degree of 67 kJ mol^{-1} and agreed with the value reported by Abe *et al*.[18] By assuming that the desolvation of TFSA anions from Li ion progresses in a stepwise fashion, and the influence of earlier desolvation on the kinetics of the interfacial Li-ion

transfer is relatively small and the last desolvation is dominant, the phenomenon which the activation energy remained unchanged can be explained. On the other hand, the solvation number of PC molecules per Li ion was about 3.8 (Fig. S7, ESI†); nevertheless the activation energy obtained from the organic electrolyte of 1 M LiTFSA-dissolved in PC resulted in the most smallest value of 49 kJ mol^{-1} among the three kind of electrolytes and gave close agreement with the value reported by Doi *et al*.[34] These experimental results again remind us that the interaction between Li ion and TFSA anions is much higher than that between Li ion and molecular solvents in the organic electrolyte, and the electrostatic interaction generated in the ionic liquid electrolytes is responsible for the slow kinetics of the interfacial Li-ion transfer. From the Raman analysis, it was revealed that the solvation numbers of TFSA anions per Li ion were 1.56 for PP1MEM-TFSA and 2.40 for PP16-TFSA, which indicate that Li ions in PP1MEM-TFSA are relatively free from the constraint generated by the electrostatic interaction, and transport ability of the Li-ion in PP1MEM-TFSA was enhanced. Based on the results, we inferred that the reason for the improved rate performance in PP1MEM-TFSA is derived from the Li-ion diffusion in the electrolyte rather than from the kinetics of the interfacial Li-ion transfer at electrode−electrolyte.[24] What these examples makes clear is that the PP1MEM cation played a key role of enhancement for Li-ion diffusion in the electrolyte bulk. An optimization of not only the cation but also anion would realize Li-ion batteries with a high energy density and a high safety.

4. Conclusions

The transport ability and solvation environment for Li ion in piperidinium-based ionic liquid electrolytes were investigated by EIS technique and Raman spectroscopic measurements. In

addition, the effect of cation structure of ionic liquid on the kinetics of interfacial Li-ion transfer between electrode and electrolyte was studied using a $Li_4Ti_5O_{12}$ thick-film prepared by gas-deposition without any binder or conductive additive. The apparent transference numbers of Li ion in PP1MEM-TFSA and PP16-TFSA were 0.32 and 0.07, respectively. Raman analysis of the electrolyte solutions revealed the following: the PP1MEM cation weakens the interaction between Li ion and TFSA anions, and thereby diminishes the solvation number of TFSA anions (N_{TFSA} 1.56) compared with that in PP16-TFSA (N_{TFSA} 2.40). When the current density was increased from 0.2 *C* to 1.0 *C*, the discharge capacity of $Li_4Ti_5O_{12}$ electrode in PP16-TFSA drastically dropped, and the electrode showed the capacity of only 40 mA h g^{-1}. On the other hand, the less solvation number in PP1MEM-TFSA enhanced the rate performance (125 mA h g^{-1} at 1.0 *C*). From the EIS measurements, it was found that the apparent activation energy associated with the interfacial Li-ion transfer showed same degree of 67 kJ mol^{-1} without depending on the cation species. This result indicates that the reason for the improved rate performance in PP1MEM-TFSA originates from not the kinetics of the interfacial Li-ion transfer at electrode−electrolyte but from the enhanced Li-ion diffusion in the electrolyte bulk.

Acknowledgments

M. Shimizu thanks Japan Society for the Promotion of Science (JSPS) for research fellowship (No. 2611485). This work has been supported by a Grant-in-Aid for Young Scientists (B) (No. 25810141) from Scientific Research of Ministry of Education, Culture, Sports, Science and Technology (MEXT) of Japan. The authors are grateful to Mr. K. Yamaguchi and Mr. N. Handa for their kind assistance for preparation of electrolyte solutions. The authors also

gratefully acknowledge Prof. Y. Domi, Prof. T. Nokami and Prof. T. Itoh for their helpful comments.

References

1. M. Armand, F. Endres, D. R. MacFarlane, H. Ohno and B. Scrosati, *Nature Mater*., 2009, **8**, 621−629.
2. D. M. Piper, T. Evans, K. Leung, T. Watkins, J. Olson, S. C. Kim, S. S. Han, V. Bhat, K. H. Oh, D. A. Buttry and S. H. Lee, *Nature Commun*., 2015, **6**, 6230.
3. H. Matsumoto, H. Sakaebe and K. Tatsumi, *J. Power Sources*, 2005, **146**, 45−50.
4. H. Sakaebe, H. Matsumoto and K. Tatsumi, *J. Power Sources*, 2005, **146**, 693−697.
5. H. Matsumoto, H. Sakaebe, K. Tatsumi, M. Kikuta, E. Ishiko and M. Kono, *J. Power Sources*, 2006, **160**, 1308−1313.
6. S. Tsuzuki, W. Shinoda, M. Matsugami, Y. Umebayashi, K. Ueno, T. Mandai, S. Seki, K. Dokko and M. Watanabe, *Phys. Chem. Chem. Phys*., 2014, **17**, 126−129.
7. K. Yoshida, M. Nakamura, Y. Kazue, N. Tachikawa, S. Tsuzuki, S. Seki, K. Dokko and M. Watanabe, *J. Am. Chem. Soc*., 2011, **133**, 13121−13129.
8. K. Tsunashima and M. Sugiya, *Electrochem. Commun*., 2007, **9**, 2353−2358.
9. K. Tsunashima, Y. Ono and M. Sugiya, *Electrochim. Acta*, 2011, **56**, 4351−4355.
10. T. Sugimoto, Y. Atsumi, M. Kikuta, E. Ishiko, M. Kono and M. Ishikawa, *J. Power Sources*, 2009, **189**, 802−805.
11. A. Lewandowski and A. Świderska-Mocek, *J. Power Sources*, 2009, **194**, 601−609.
12. R. Furuya, N. Tachikawa, K. Yoshii, Y. Katayama and T. Miura, *J. Electrochem. Soc*., 2015, **162**, H634−H637.

13. J.-W. Song, C. C. Nguyen and S.-W. Song, *RSC Adv*., 2012, **2**, 2003−2009.
14. N. Yabuuchi, K. Shimomura, Y. Shimbe, T. Ozeki, J.-Y. Son, H. Oji, Y. Katayama, T. Miura and S. Komaba, *Adv. Energy Mater*., 2011, **1**, 759−765.
15. V. Chakrapani, F. Rusli, M. A. Filler and P. A. Kohl, *J. Phys. Chem. C*, 2011, **115**, 22048−22053.
16. H. Usui, M. Shimizu and H. Sakaguchi, *J. Power Sources*, 2013, **235**, 29−35.
17. F. Sagane, T. Abe and Z. Ogumi, *J. Electrochem. Soc*., 2012, **159**, A1766−A1769.
18. Y. Ishihara, K. Miyazaki, T. Fukutsuka and T. Abe, *J. Electrochem. Soc*., 2014, **161**, A1939−A1942.
19. M. Shimizu, H. Usui, K. Matsumoto, T. Nokami, T. Itoh and H. Sakaguchi, *J. Electrochem. Soc*., 2014, **161**, A1765−A1771.
20. M. Egashira, A. Kanetomo, N. Yoshimoto and M. Morita, *J. Power Sources*, 2011, **196**, 6419−6424.
21. Y. Umebayashi, S. Mori, K. Fujii, S. Tsuzuki, S. Seki, K. Hayamizu, and S. Ishiguro, *J. Phys. Chem. B*, 2010 **114**, 6513−6521.
22. J. C. Lassègues, J. Grondin and D. Talaga, *Phys. Chem. Chem. Phys*., 2006, **8**, 5629−5632.
23. Y. Katayama, R. Fukui and T. Miura, *J. Electrochem. Soc*., 2007, **154**, D534−D537.
24. K. Yoshida, M. Tsuchiya, N. Tachikawa, K. Dokko, M. Watanabe, *J. Electrochem. Soc*., 2012, **159**, A1005−A1012.
25. M. Shimizu, H. Usui, T. Suzumura and H. Sakaguchi, *J. Phys. Chem. C*, 2015, **119**, 2975−2982.
26. B. Baek, S. Lee, and C. Jung, *Int. J. Electrochem. Sci*., 2011, **6**, 6220−6234.
27. T. Ohzuku, A. Ueda and N. Yamamoto, *J. Electrochem. Soc*., 1995, **142**, 1431−1435.

28. Y. H. Rho and K. Kanamura, *J. Solid State Chem*., 2004, **177**, 2094−2100.

29. L. Aldon, P. Kubiak, M. Womes, J. C. Jumas, J. Olivier-Fourcade, J. L. Tirado, J. I. Corredor, C. P. Vicente, *Chem. Mater*., 2004, **16**, 5721−5725.

30. J. Haetge, P. Hartmann, K. Brezesinski, J. Janek and T. Brezesinski, *Chem. Mater*., 2011, **23**, 4384−4393.

31. H.-G. Jung, S.-T. Myung, C. S. Yoon, S.-B. Son, K. H. Oh, K. Amine, B. Scrosati and Y.-K. Sun, *Energy Environ. Sci*., 2011, **4**, 1345−1351.

32. T. Abe, H. Fukuda, Y. Iriyama and Z. Ogumi, *J. Electrochem. Soc*., 2004, **151**, A1120−A1123.

33. Y. Yamada, Y. Iriyama, T. Abe and Z. Ogumi, *Langmuir*, 2009, **25**, 12766−12770.

34. T. Doi, Y. Iriyama, T. Abe and Z. Ogumi, *Anal. Chem*., 2005, **77**, 1696−1700.

35. T. Nokami, K. Matsumoto, T. Itoh, Y. Fukaya and T. Itoh, *Org. Process Res. Dev*., 2014, **18**, 1367−1371.

36. M. Shimizu, H. Usui and H. Sakaguchi, *J. Power Sources*, 2014, **248**, 378−382.

37. J. Evans, C. A. Vincent and P. G. Bruce, *Polymer*, 1987, **28**, 2324−2328.

38. S. Seki, Y. Ohno, H. Miyashiro, Y. Kobayashi, A. Usami, Y. Mita, N. Terada, K. Hayamizu, S. Tsuzuki and M. Watanabe, *J. Electrochem. Soc*, 2008, **155**, A421−A427.

39. K. Matsumoto, Y. Okamoto, T. Nohira and R. Hagiwara, *J. Phys. Chem. C*, 2015, **119**, 7648−7655.

40. Y. Umebayashi, T. Mitsugi, S. Fukuda, T. Fujimori, K. Fujii, R. Kanzaki, M. Takeuchi and S. Ishiguro, *J. Phys. Chem. B*, 2007, **111**, 13028−13032.

41. K. Xu, A. von Cresce and U. Lee, *Langmuir*, 2010, 26, 11538−11543.

42. S. Duluard, J. Grondin, J.-L. Bruneel, I. Pianet, A. Grélard, G. Campet, M.-H. Delville and J.-C. Lassègues, *J. Raman Spectrosc*., 2008, **39**, 627−632.

43. S. Menne, T. Vogl and A. Balducci, *Phys. Chem. Chem. Phys*., 2014, **16**, 5485−5489.

44. M. Kunze, S. Jeong, E. Paillard, M. Schönhoff, M. Winter and S. Passerini, *Adv. Energy Mater*., 2011, **1**, 274−281.

45. S. Tsuzuki, K. Hayamizu, S. Seki, Y. Ohno, Y. Kobayashi and H. Miyashiro, *J. Phys. Chem. B*, 2008, **112**, 9914−9920.

Figure captions

Fig. 1 Cation and anion structures of ionic liquids used in this study.

Fig. 2 Impedance spectra of [Li metal | 1 M LiTFSA/TFSA-based ionic liquid | Li metal] symmetric cells at 303 K. The cation of ionic liquids are (a) PP1MEM and (b) PP16, respectively. Polarization voltage: 10 mV. (c) Randles circuit used in this study for analysis of each cell impedance. (d) Time dependence of dc currents for the symmetric cell at 303 K.

Fig. 3 Deconvoluted Raman bands of (a) $(LiTFSA)_x(PP1MEM\text{-}TFSA)_{1-x}$ and (b) $(LiTFSA)_x(PP16\text{-}TFSA)_{1-x}$ solutions. The black, dotted, red, and blue lines correspond to the observed spectrum, the total Raman spectrum, the deconvoluted components of *free* TFSA anions ($TFSA^-_{free}$) and TFSA anions interacting with Li^+ ($TFSA^-_{solv}$).

Fig. 4 Plot of I_{solv} / (I_{free}+ I_{solv}) as a function of x for $(LiTFSA)_x(PP1MEM\text{-}TFSA)_{1-x}$ and $(LiTFSA)_x(PP16\text{-}TFSA)_{1-x}$. The dotted lines show slopes in case which an average solvation number (n) of TFSA anion per Li ion is one, two, and three. The average solvation number of TFSA anions is 1.56 for PP1MEM-TFSA system and 2.40 for PP16-TFSA system.

Fig. 5 (a) XRD pattern and (b) Raman spectrum of $Li_4Ti_5O_{12}$ thick-film electrode prepared by a gas-deposition method. FE-SEM image of $Li_4Ti_5O_{12}$ powder used in this study is inserted. (c) Optical image of the $Li_4Ti_5O_{12}$ electrode and three-dimensional height profile analyzed by a confocal scanning laser microscope. The deposited film thickness is *ca*. 36 mm.

Fig. 6 Rate capability of $Li_4Ti_5O_{12}$ thick-film electrodes in piperidinium-based ionic liquid electrolytes at various *C*-rates from 0.1 *C* (17.5 mA g^{-1}) to 20 *C* (3500 mA g^{-1}). For comparison, the performance in the organic electrolyte of 1 M LiTFSA/PC was also plotted.

Fig. 7 Charge−discharge profiles of $Li_4Ti_5O_{12}$ thick-film electrodes at 0.5 *C* rate in ionic liquid electrolyte of (a) PP1MEM-TFSA, (b) PP16-TFSA, and (c) PC.

Fig. 8 (a) Typical Nyquist plot and the result of fitting by equivalent circuits for impedance analysis. (b) Nyquist plots of $Li_4Ti_5O_{12}$ thick-film electrodes charged at 1.55 V vs. Li/Li^+ the first cycle in PP1MEM-TFSA and PP16-TFSA at 303 K. (c) Temperature dependence of interfacial resistance of the electrodes in the electrolyte of 1 M LiTFSA-dissolved in PP1MEM-TFSA, PP16-TFSA and PC. Activation energies were obtained from the slope.

Table 1 Summary of measured values for the parameters and apparent transference number of Li^+ (t_{Li+}) obtained from impedance analysis for the [Li metal | 1 M LiTFSA/TFSA-based ionic liquid | Li metal] symmetric cells at 303 K. Polarization voltage:10 mV.

Cation	i_0 (μA)	i_0 (μA)	$R_{(0)\,bulk}$ (Ω)	$R_{(\infty)\,bulk}$ (Ω)	$R_{(0)lithium}$ (Ω)	$R_{(\infty)lithium}$ (Ω)	t_{Li+}
PP1MEM	26.2	17.3	20.5	21.5	300	312	0.32
PP16	21.4	7.27	54.0	56.0	405	475	0.07

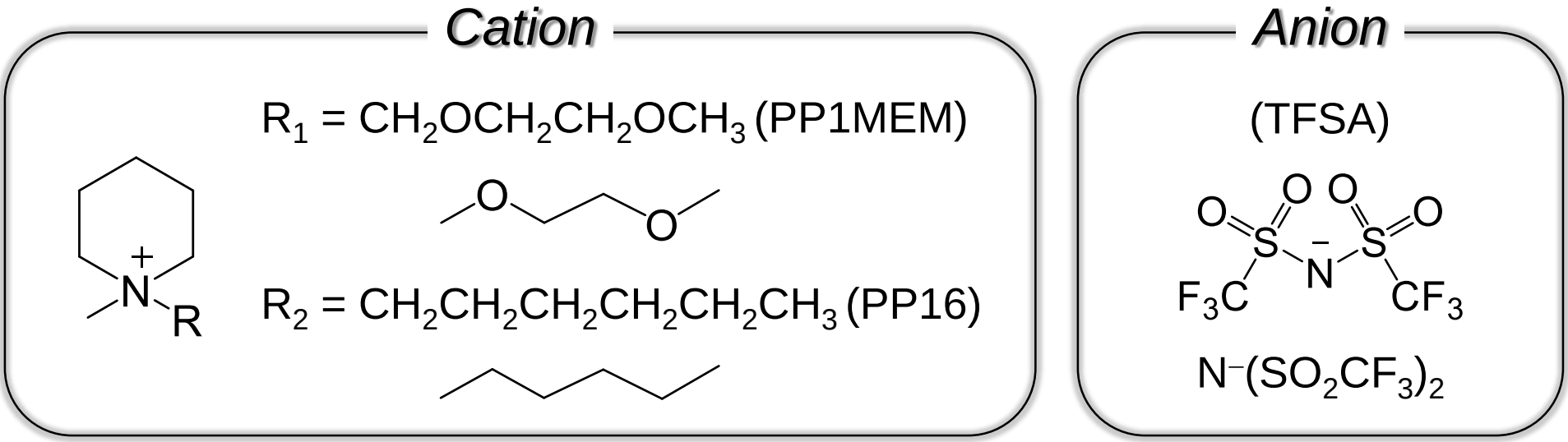

PP1MEM : 1-((2-methoxyethoxy)methyl)-1-methylpiperidinium
PP16 : 1-hexyl-1-methylpiperidinium
TFSA : bis(trifluoromethanesulfonyl)amide

Figure 1. Cation and anion structures of ionic liquids used in this study.

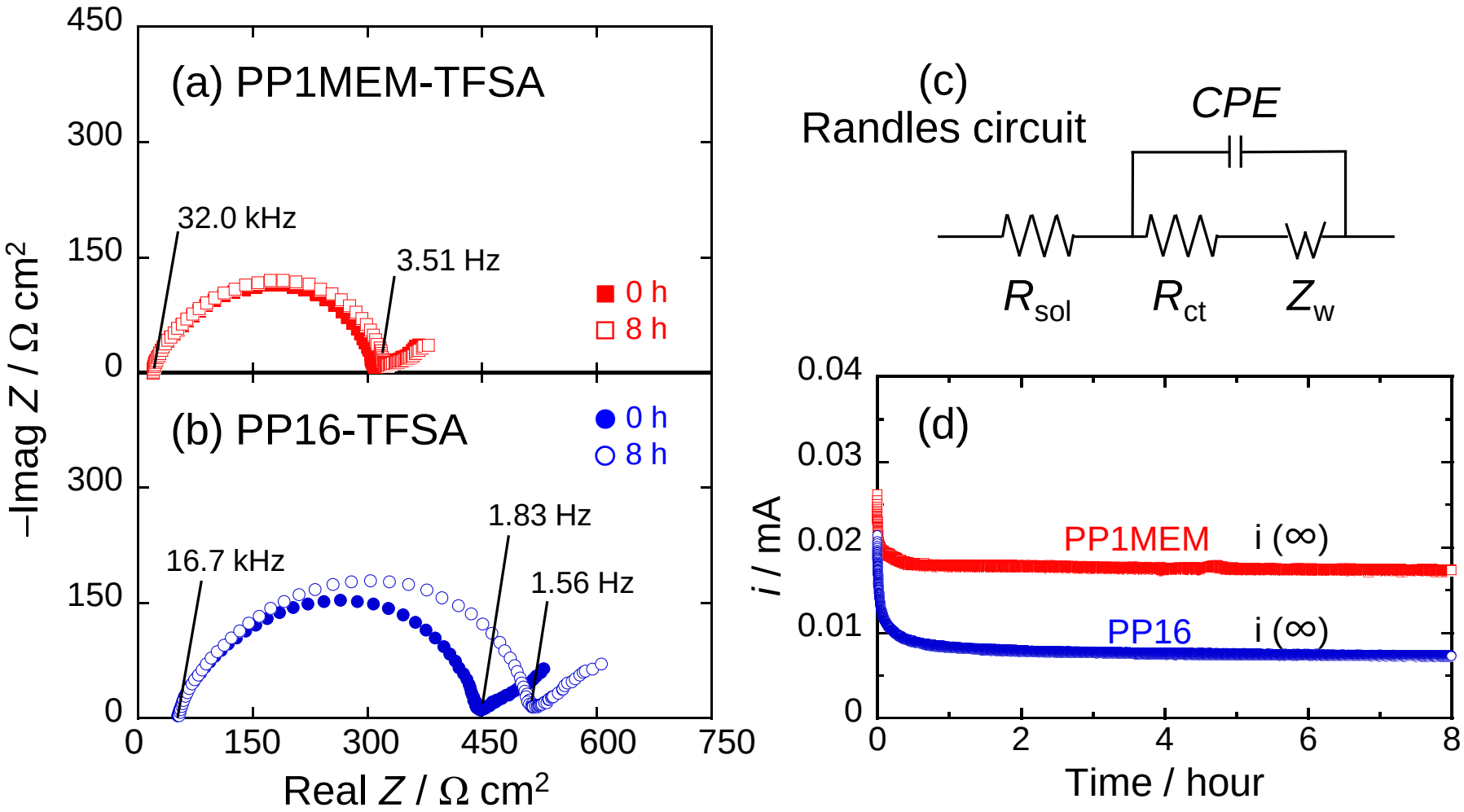

Figure 2. Impedance spectra of [Li metal | 1 M LiTFSA/TFSA-based ionic liquid | Li metal] symmetric cells at 303 K. The cation of ionic liquids are (a) PP1MEM and (b) PP16, respectively. Polarization voltage: 10 mV. (c) Randles circuit used in this study for analysis of each cell impedance. (d) Time dependence of dc currents for the symmetric cell at 303 K.

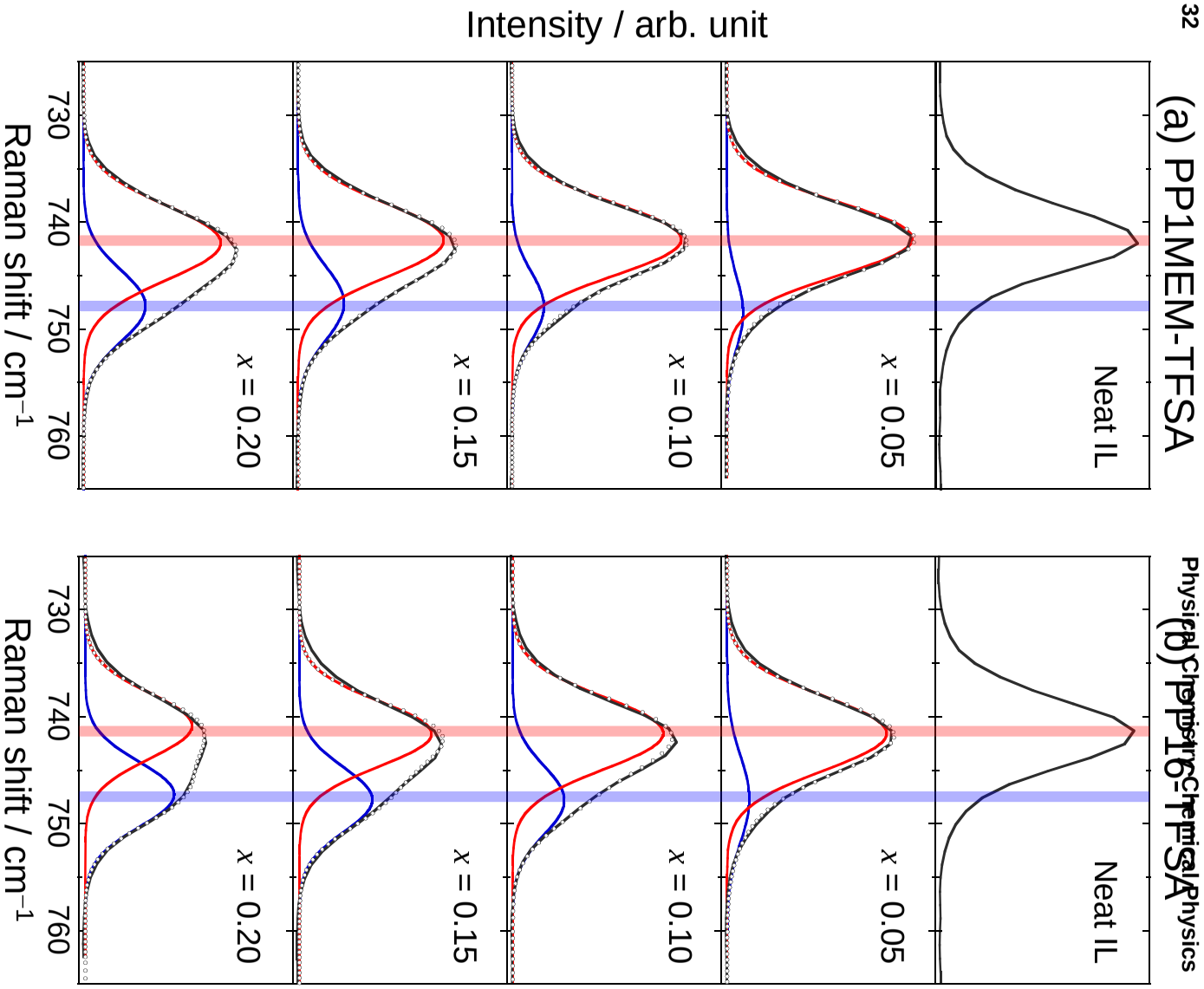

Figure 3. Deconvoluted Raman bands of (a) $(LiTFSA)_x(PP1MEM\text{-}TFSA)_{1-x}$ and (b) $(LiTFSA)_x(PP16\text{-}TFSA)_{1-x}$ solutions. The black, dotted, red, and blue lines correspond to the observed spectrum, the total Raman spectrum, the deconvoluted components of *free* TFSA anions ($TFSA^-_{free}$) and TFSA anions interacting with Li^+ ($TFSA^-_{solv}$).

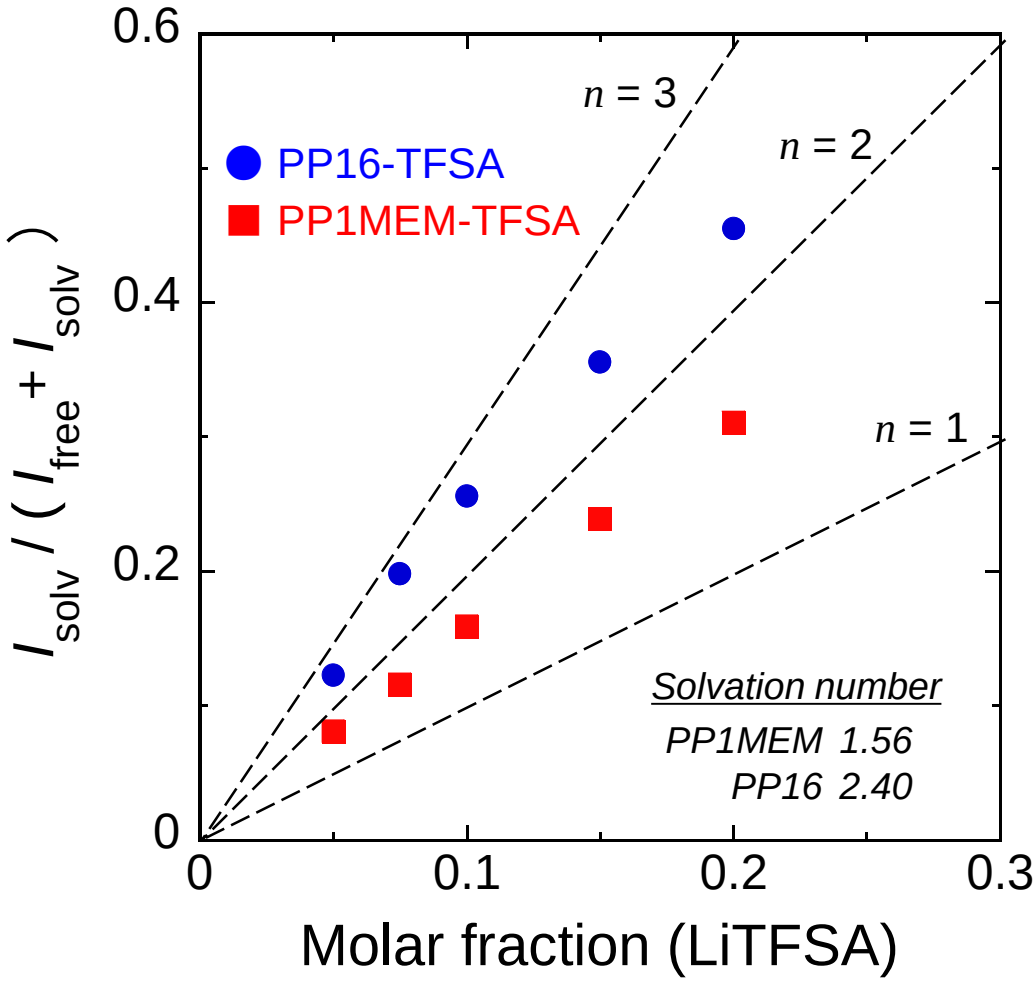

Figure 4. Plot of I_{solv} / (I_{free}+ I_{solv}) as a function of x for $(LiTFSA)_x(PP1MEM\text{-}TFSA)_{1-x}$ and $(LiTFSA)_x(PP16\text{-}TFSA)_{1-x}$. The dotted lines show slopes in case which an average solvation number (n) of TFSA anion per Li ion is one, two, and three. The average solvation number of TFSA anions is 1.56 for PP1MEM-TFSA system and 2.40 for PP16-TFSA system.

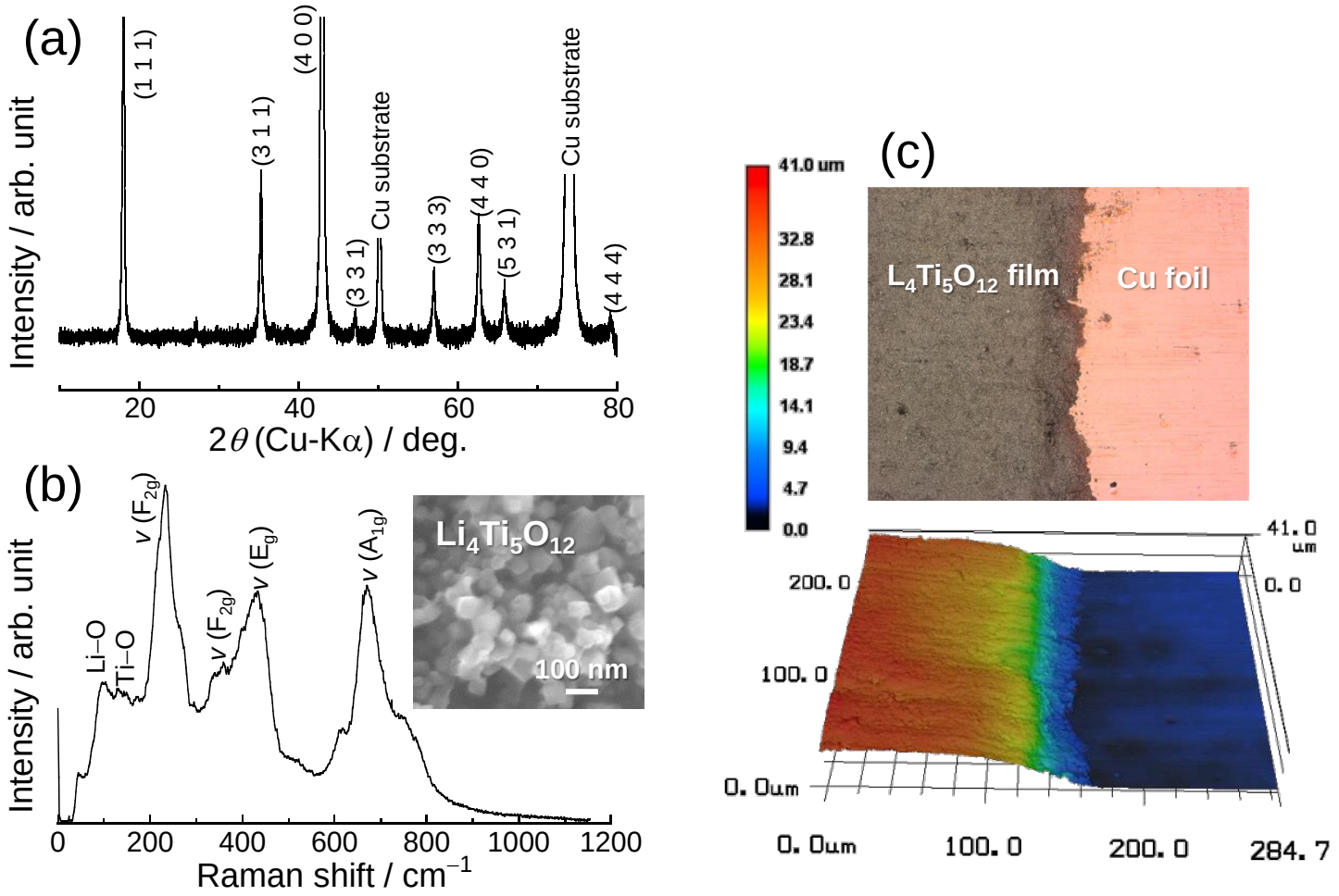

Figure 5. (a) XRD pattern and (b) Raman spectrum of $Li_4Ti_5O_{12}$ thick-film electrode prepared by a gas-deposition method. FE-SEM image of $Li_4Ti_5O_{12}$ powder used in this study is inserted. (c) Optical image of the $Li_4Ti_5O_{12}$ electrode and three-dimensional height profile analyzed by a confocal scanning laser microscope. The deposited film thickness is *ca*. 36 μm.

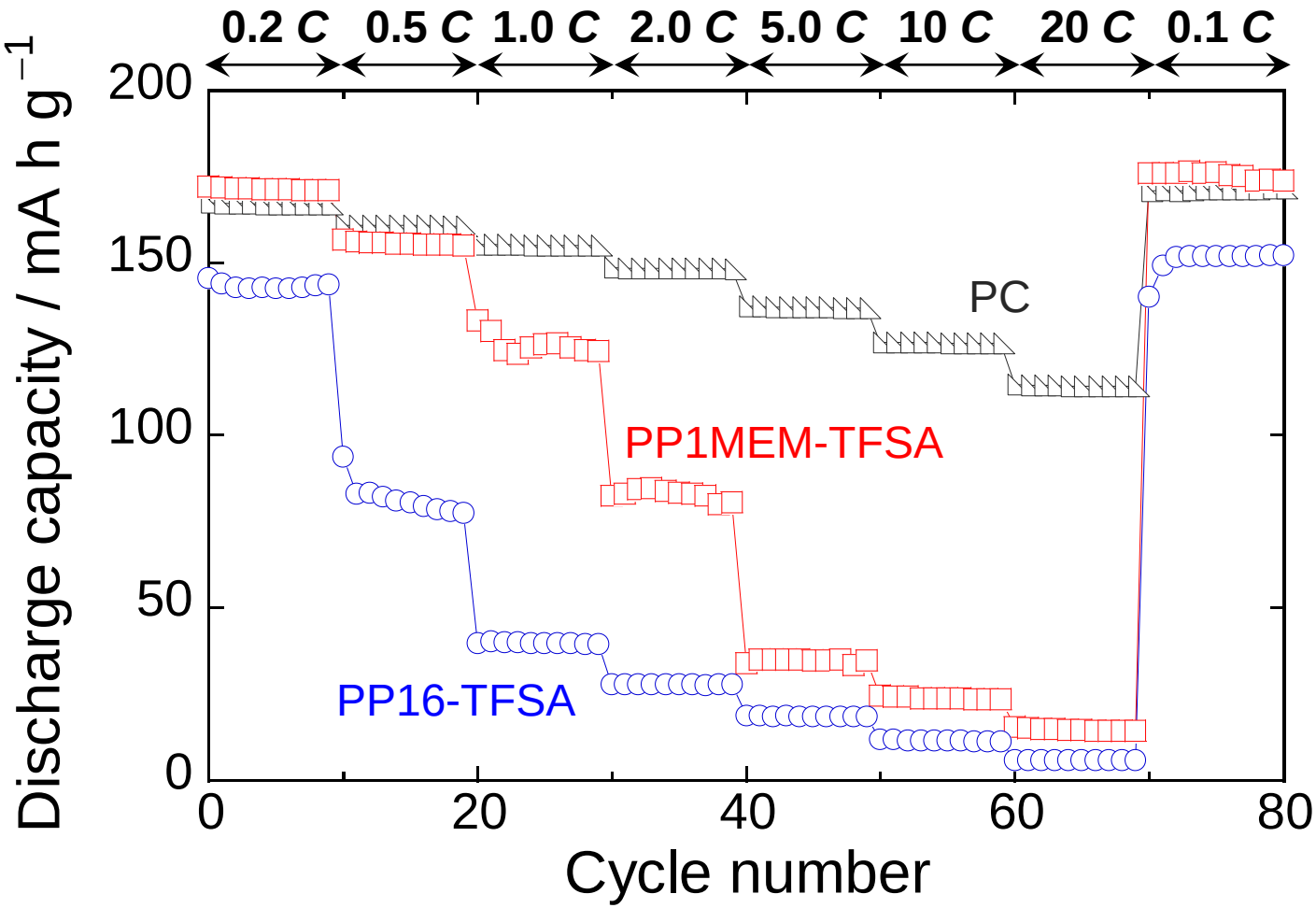

Figure 6. Rate capability of $Li_4Ti_5O_{12}$ thick-film electrodes in piperidinium-based ionic liquid electrolytes at various *C*-rates from 0.1 *C* (17.5 mA g^{-1}) to 20 *C* (3500 mA g^{-1}). For comparison, the performance in the organic electrolyte of 1 M LiTFSA/PC was also plotted.

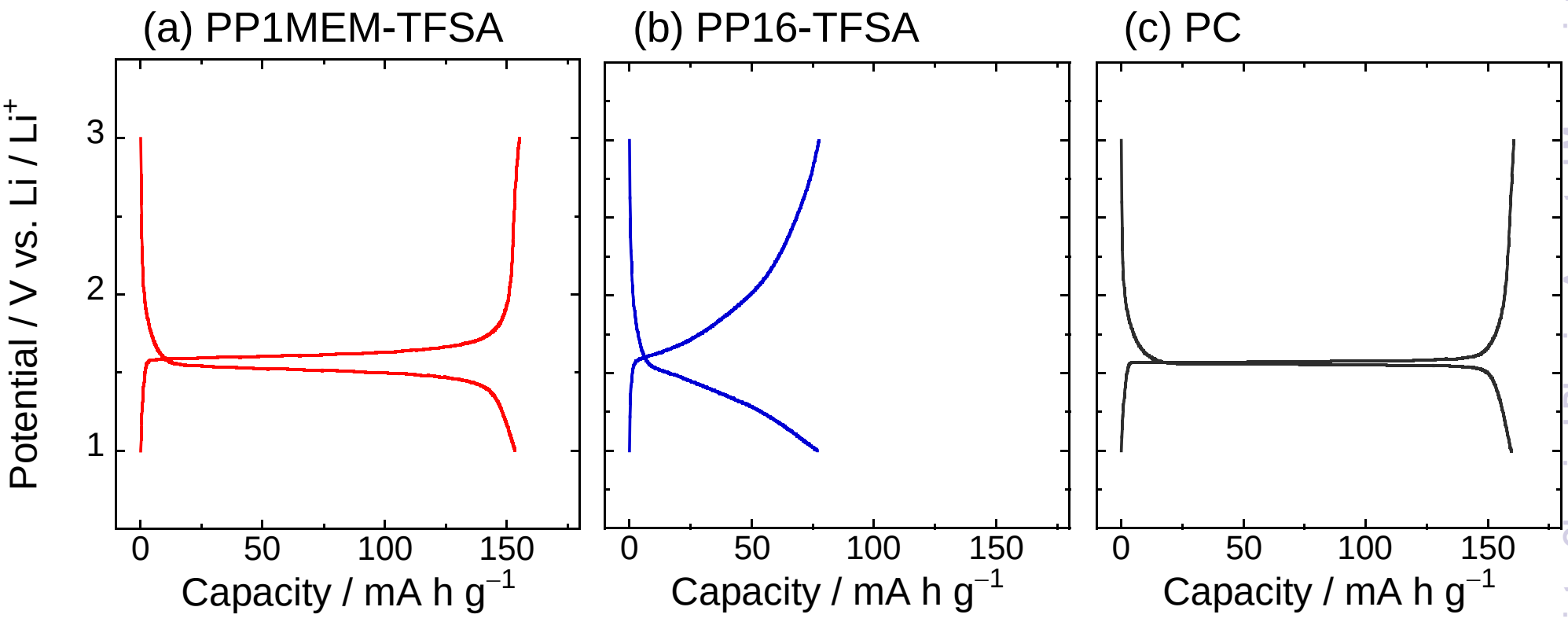

Figure 7. Charge–discharge profiles of $Li_4Ti_5O_{12}$ thick-film electrodes at 0.5 *C* rate in ionic liquid electrolyte of (a) PP1MEM-TFSA, (b) PP16-TFSA, and (c) PC.

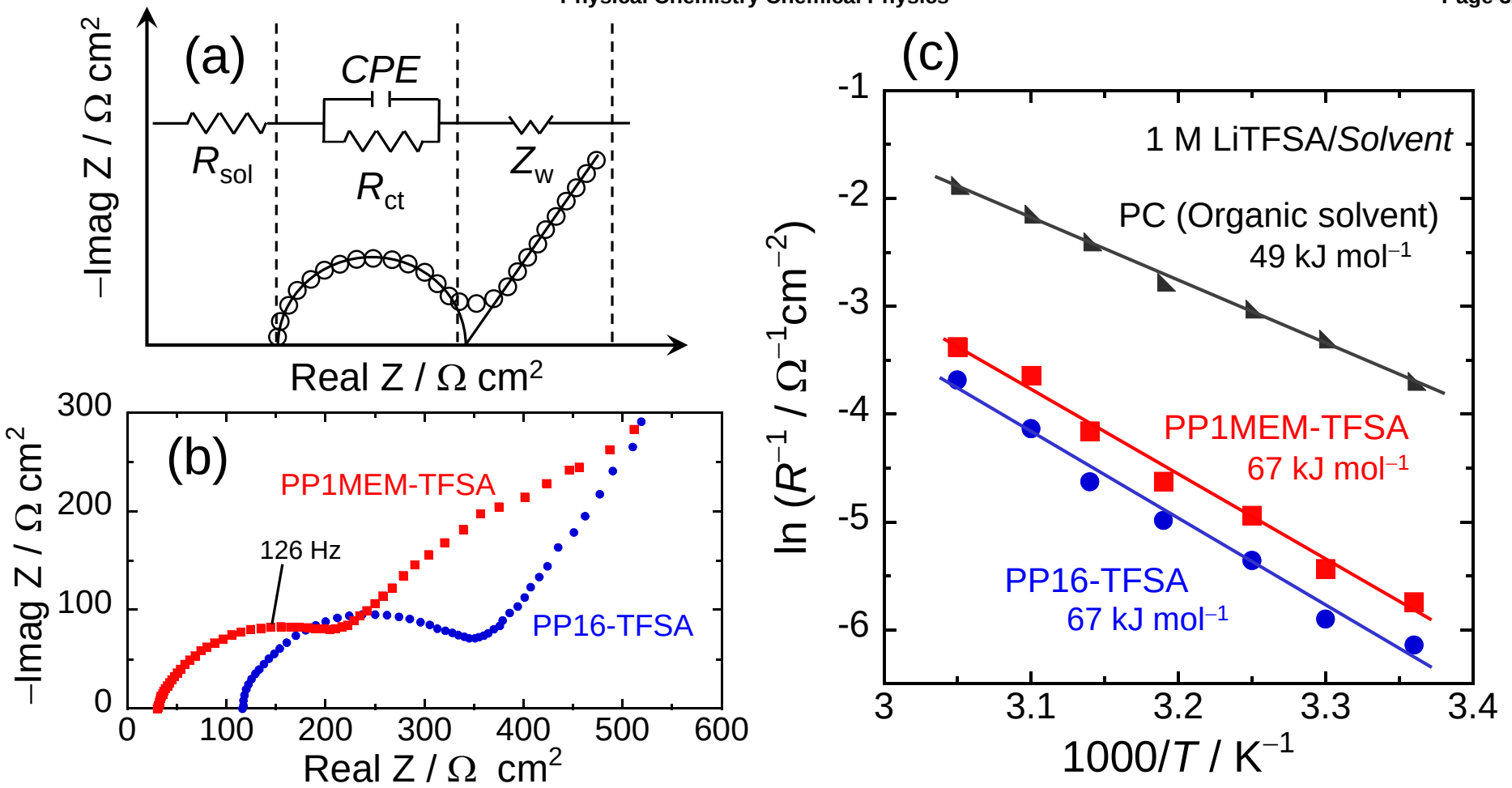

Figure 8. (a) Typical Nyquist plot and the result of fitting by equivalent circuits for impedance analysis. (b) Nyquist plots of $Li_4Ti_5O_{12}$ thick-film electrodes charged at 1.55 V vs. Li/Li^+ the first cycle in PP1MEM-TFSA and PP16-TFSA at 303 K. (c) Temperature dependence of interfacial resistance of the electrodes in the electrolyte of 1 M LiTFSA-dissolved in PP1MEM-TFSA, PP16-TFSA and PC. Activation energies were obtained from the slope.